GIG Research Institute

JOURNAL OF SUSTAINABLE MINING

Volume 22 | Issue 4 Article 3

2023

Numerical modelling of Uniaxial Compressive Strength laboratory tests

Author(s) ORCID Identifier:
Phu Minh Vuong Nguyen: 0000-0002-4895-8811
Andrzej Walentek: 0000-0003-1238-4921
Petr Waclawik: 0000-0002-9589-5083
Kamil Soucek: 0000-0002-4430-8272

Numerical modelling of Uniaxial Compressive Strength laboratory tests

Abstract

In the last decades, numerical modelling has been widely used to simulate rock mass behaviour in geo-engineering issues. The only disadvantage of numerical modelling is the reliability of required input data (e.g. mechanical parameters), which is not always fully provided due to the complexity of rock mass, project budget, available test methods or human errors. On the other hand, it was proven in many cases that numerical modelling is a helpful tool for solving such complex problems, especially when coupled with the results of laboratory and in-situ tests. This paper presents an attempt to determine the proper numerical constitutive model of rock and its mechanical parameters for further simulating rock mass response based on the outcomes of laboratory testing. For this purpose, the available constitutive models, including mechanical parameters, were taken into account. The simulation performance with the selected constitutive models is demonstrated by matching the numerical modelling results with the uniaxial compressive strength laboratory tests of rock samples from the Bogdanka coal mine. All numerical simulations were carried out using the finite difference method software FLAC3D

Keywords

Uniaxial Compressive Strength (UCS), Numerical modelling, Constitutive model, Fracture mode

Authors

Phu Minh Vuong Nguyen, Andrzej Walentek, Petr Waclawik, Kamil Soucek, and Michał Antoniuk

RESEARCH ARTICLE

Numerical modelling of uniaxial compressive strength laboratory tests

Phu Minh Vuong [a,*], Andrzej Walentek [a], Petr Waclawik [b], Kamil Souček [b], Michał Antoniuk [c]

[a] Central Mining Institute, Katowice, Poland
[b] Institute of Geonics, Czech Academy of Sciences, Ostrava, Czech Republic
[c] Bogdanka Coal Mnie, Puchaczów, Poland

Abstract

In the last decades, numerical modelling has been widely used to simulate rock mass behaviour in geo-engineering issues. The only disadvantage of numerical modelling is the reliability of required input data (e.g. mechanical parameters), which is not always fully provided due to the complexity of rock mass, project budget, available test methods or human errors. On the other hand, it was proven in many cases that numerical modelling is a helpful tool for solving such complex problems, especially when coupled with the results of laboratory and in-situ tests. This paper presents an attempt to determine the proper numerical constitutive model of rock and its mechanical parameters for further simulating rock mass response based on the outcomes of laboratory testing. For this purpose, the available constitutive models, including mechanical parameters, were taken into account. The simulation performance with the selected constitutive models is demonstrated by matching the numerical modelling results with the uniaxial compressive strength laboratory tests of rock samples from the Bogdanka coal mine. All numerical simulations were carried out using the finite difference method software FLAC3D.

Keywords: uniaxial compressive strength (UCS), numerical modelling, constitutive model, fracture mode

1. Introduction

The Uniaxial Compressive Strength (UCS) test is one of the most common procedures to directly define the intact rock strength, Young's modulus and Poisson ratio [1–4]. The failure modes in this test have been explained and hypothesised in compliance with damage evolution, such as micro-crack generation [5–11], propagation [12–14] and coalescence [15,16] in rocks under uniaxial compression. It should be noted that it was impossible to capture complete fracture mode leading to specimen failure under uniaxial compression due to the limit of specimens and type of geo-material. Further studies should be considered in order to verify the hypothesis more objectively than a single experimental study using a sophisticated real-time device.

With the rapid advance in computer science and numerical modelling, a number of studies have been carried out to simulate the laboratory tests to understand the characteristics of rock mass behaviour. Authors have employed various numerical methods and numerical constitutive models to simulate various geo-materials given under the uniaxial compression tests. A brief summary of case studies is drawn in Table 1.

It can be noted that the constitutive model and its parametric components, which represent the geo-material behaviour, have played a key role in modelling of the uniaxial compression strength tests.

This paper presents an attempt to implement the uniaxial compression test simulation. Initially, the mesh quality analysis were conducted to define the mesh number of zones, and the mesh pattern suitable for further analysis. Subsequently, the selected built-in constitutive models available in the software FLAC3D [33] were simulated. The results were

Received 31 March 2023; revised 10 May 2023; accepted 20 May 2023.
Available online 21 September 2023

* Corresponding author.
E-mail address: pnguyen@gig.eu (P.M. Vuong).

https://doi.org/10.46873/2300-3960.1393

Table 1. Numerical studies on the compressive tests of rock samples.

Author, year	Type of numerical code	Application note
Stefanizzi et al., 2009 [17]	2D ELFEN (the explicit finite element method-based)	Modelling of compressive tests of rock samples (an idealized homogeneous isotropic rock)
Mahabadi et al., 2014 [18]	3D FDEM (hybrid finite-discrete element method)	Modelling of development of the excavation damaged zone (EDZ) around tunnels in a clay shale formation
Tatone and Grasselli, 2015 [19]	Combined finite/discrete element method (FEM–DEM)	Modelling of the brittle fracture process in geo-materials (flowstone mortar material) for the uniaxial compressive test
Mardalizad et al., 2018 [20]	Finite element method coupled smooth particle hydrodynamics technique (in LS-DYNA)	Numerical simulation of the unconfined compression test of sandstone sample with an advanced material model (Karagozian-Case Concrete model)
Xiong et al., 2019 and 2021 [21,22]	Different element method software FLAC3D	Numerical modelling on artificial jointed rock samples with two parallel equal-length joint fractures to study the strength characteristics of jointed rock mass (classic Mohr-Coulomb model)
Oliveira et al., 2020 [23]	Hybrid numerical models (Finite/discrete element methods)	Modelling of transition from continuous to discontinuous of physical laboratory tests of andesites
Pająk et al., 2021 [24]	3D meso-scale modelling	Numerical investigations of three types of self-compacting concrete in Split Hopkinson Pressure Bar compression tests (Johnson-Holmquist constitutive model)
Kucewicz et al., 2020 and 2021 [25,26]	Finite element method (FEM) hydrocode LS-DYNA	Simulation of dolomite rock using the Johnson-Holmquist constitutive model and Karagozian-Case Concrete constitutive model
Li and Wong, 2012; Yang et al., 2014; Bahaaddini et al., 2014; Zhao et al., 2015; Haeri et al., 2019; Zhang et al., 2020; Ma et al., 2022 [27–32]	Particle Flow Code	Uniaxial compression numerical simulation of marble, red sandstone, and rock-like material with joints specimens

analysed by comparing them with the indoor tests' results to define the proper constitutive model for further simulating rock mass response. As a final result, an appropriate material model and its component parameters can be determined for further modelling analysis of rock mass response.

2. Laboratorial uniaxial compression test

2.1. Method and test equipment

The methodologies of determination of physico-mechanical properties were based on common technical norms (ČSN-EN-1926) [34] and the International Society for Rock Mechanic – ISRM [1,2]. Standard laboratory device equipment was used for the determination of physico-mechanical properties. The compressive strengths and deformation properties of rocks were determined by the ZWICK 1494 mechanical press machine with a special load cell. The LVDT (Linear Variable Displacement Transformer) sensor is installed in the load cell. Four sensors are used to measure longitudinal deformation, and eight to measure transversal deformation (Fig. 1).

2.2. Selection and preparation of sample materials

The geotechnical station was located in the longwall panel G6 within the overlying strata of coal seam No. 385 at the Bogdanka coal mine. The G6 longwall panel equipped with the plough technology was situated at a depth of 875–920 m below the surface. The extracted coal seam thickness varied from 1.15 to 1.5 m. The rock mass was characterised using exploratory borehole No. BR-59/20 before installation of the geotechnical station. The average RQD parameter value determined from the whole footage of the BR-59/20 borehole reaches only 34%, which is practically "poor" rock quality in terms of the classification by Deere [35,36]. The siltstone predominates in the overlying strata of coal seam No. 385. Coal or sandstone are represented only locally. The character of the rock mass and its quality is shown in Fig. 2.

Due to the poor quality of the rock mass, the choice of drilled core for the preparation of testing samples was limited. The length of cylindrical samples was then adjusted to the required dimension of testing samples; the bases were sharpened. Bodies with a slenderness ratio of 2:1 were used for

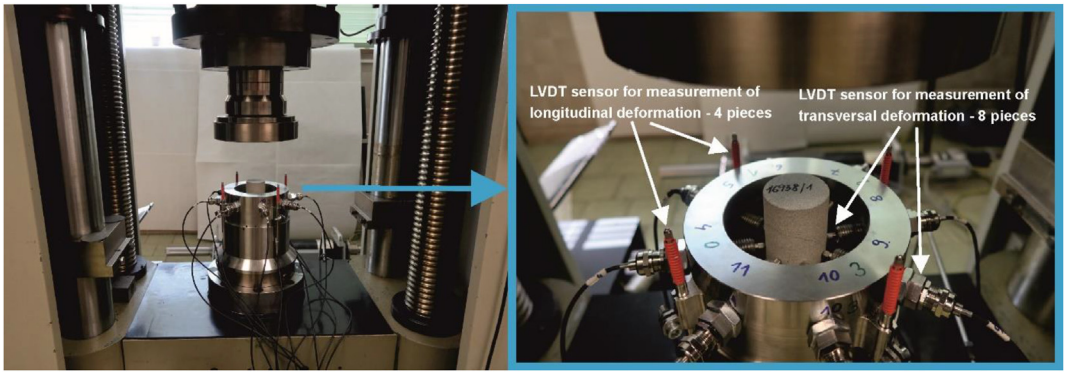

Fig. 1. Mechanical press machine with a load cell.

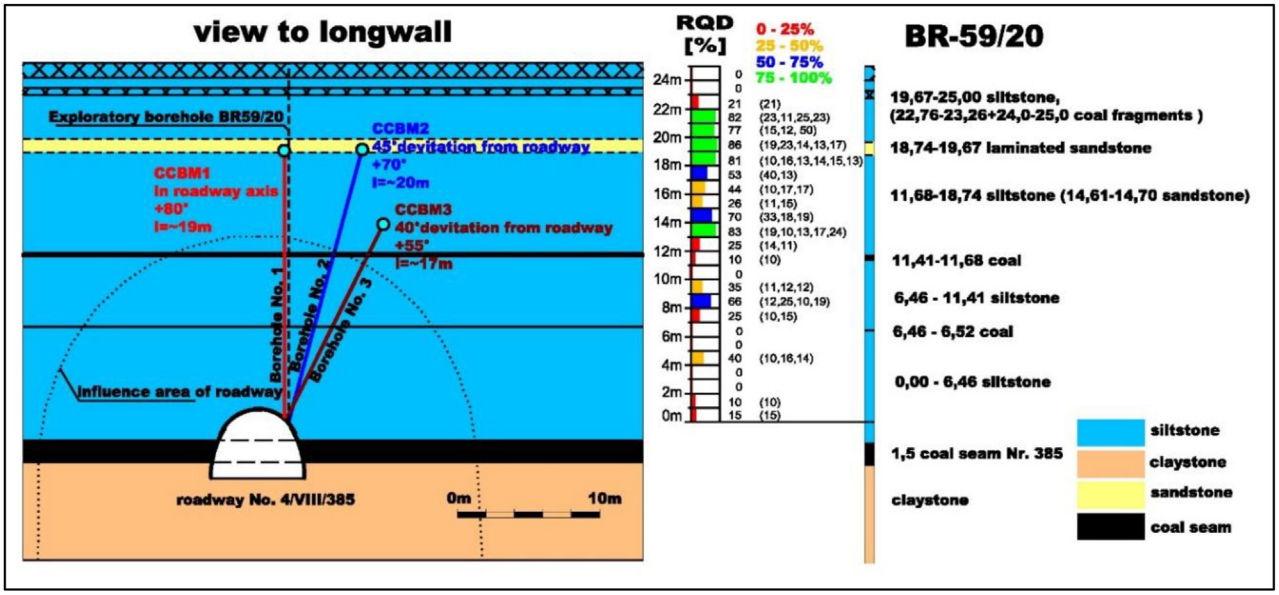

Fig. 2. The rock mass characterisation of the geotechnical station GS1.

the determination of uniaxial compressive strength. The testing samples were dried at 105 °C to stabilised humidity and then a uniaxial compressive test were performed.

2.3. Test results

The results of mechanical properties determination are presented in the following Table 2. An absolute majority of tested intact testing samples exhibits the uniaxial compressive strength in the range of 35–80 MPa. Therefore overlying rocks of coal seam No. 385 at the Bogdanka coal mine can be classified into classes of rocks with a moderate to medium strength (average 62 MPa) in terms of known strength classifications [37,38]. The uniaxial compressive strength exceeds 100 MPa for only one testing sample (16–914/1). These samples have a different lithological composition, containing fine-grained sandstone and sandy siltstone. Typical failure-deformation characteristics are shown in Fig. 3.

From the visual comparison of testing samples, it can be concluded that the values of uniaxial compressive strength and Young's modulus depend on the samples' composition and the orientation of

Table 2. Results of testing samples.

Testing sample No.	*UCS* [MPa]	E_{sec50} [MPa]	μ_{sec50} [-]
16-914/1	111	32,043	0.13
16-914/2	63	18,187	0.09
16–915	59	20,062	0.09
16-916/1	32	19,976	0.17
16-916/2	47	22,242	0.11
Arithmetic mean	**62**	**22,502**	**0.12**
Standard deviation	27	4941	0.03

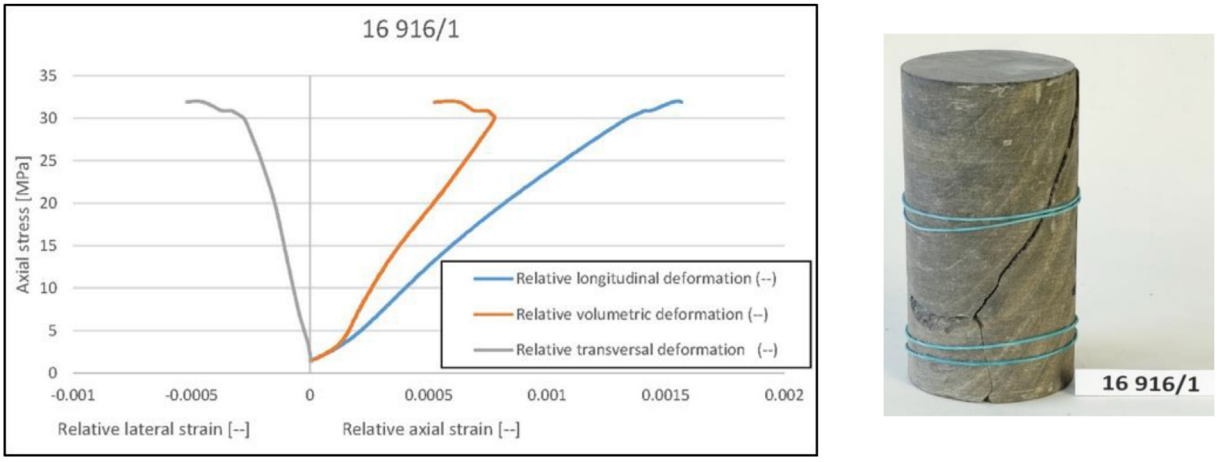

Fig. 3. Results of the uniaxial compressive test for the 16–916/1 sample.

the lamination to the test loading. The values of the Poisson ratio reach an average of 0.10.

3. Numerical analysis

In this study, a finite difference method software FLAC3D [33] was employed to model Uniaxial Compressive Strength (*UCS*) laboratory tests. Numerical models represent the geometry of actual samples mentioned in chapter 2. Cylindrical samples with a height-to-diameter ratio of 2:1 (h = 122 mm and d = 61 mm) were used for the uniaxial compression test. All numerical models were fixed at the bottom in appropriate directions (perpendicular to individual planes). The models were originally developed as elastic to achieve the primary stress state (pre-loading state). Then the displacements and velocity vectors were zeroed. In the next step, a uniform velocity is applied at the top of the cylindrical sample, moving down in the longitudinal direction to induce compression of the sample.

3.1. Mesh quality assessment

High-quality meshes are often required for the accuracy and reliability of results in numerical simulations. A number of studies have been carried out to determine the proper mesh quality metrics [39–44]. These studies indicated the importance of the mesh's high-resolution and well-shaped on the final result accuracy. However, the design of finite difference meshes for solving three-dimensional problems is always a compromise between accuracy and computation time. Hence, a mesh sensitivity analysis was performed. To capture the effects of the element number and shapes on the final results, the sample modelling was calculated with two mesh patterns with the average zone length set to 10, 5, 3 and 1.5 mm. Two mesh patterns (I – Primitive mesh shape and II – Modified mesh shape) are shown in Fig. 4. Primitive mesh shape is an approach to grid generation in FLAC3D that involves patching together grid shapes of specific connectivity to form a complete model with the required geometry (wedges and bricks). A modified (manually) mesh shape is used to be formed in the other software programs and then imported to FLAC3D (only bricks).

The number of zones due to mesh patterns and the average zone length is shown in Table 3.

A comparison of the compressive strength value due to the mesh pattern and the average zone length is presented in Table 4. Relative errors indicate the slight effect of a number of zones on the yield strength value. Relative errors in the case of mesh pattern II were lower than the ones in case of mesh pattern I. It confirms the well-known statement: in terms of accuracy, a structured hexahedral mesh usually results in the best-shaped elements.

The final model should be designed in the form of mesh pattern II. The average zone length for further analysis was set to 3 mm (Fig. 5). This value can be considered as a compromise between accuracy and time calculation.

3.2. Selection of material models for testing sample – constitutive models

Numerical solution schemes in FLAC3D face several difficulties when implementing constitutive models to represent geomechanical material behaviour. There are three characteristics of geomaterials that cause particular problems: the

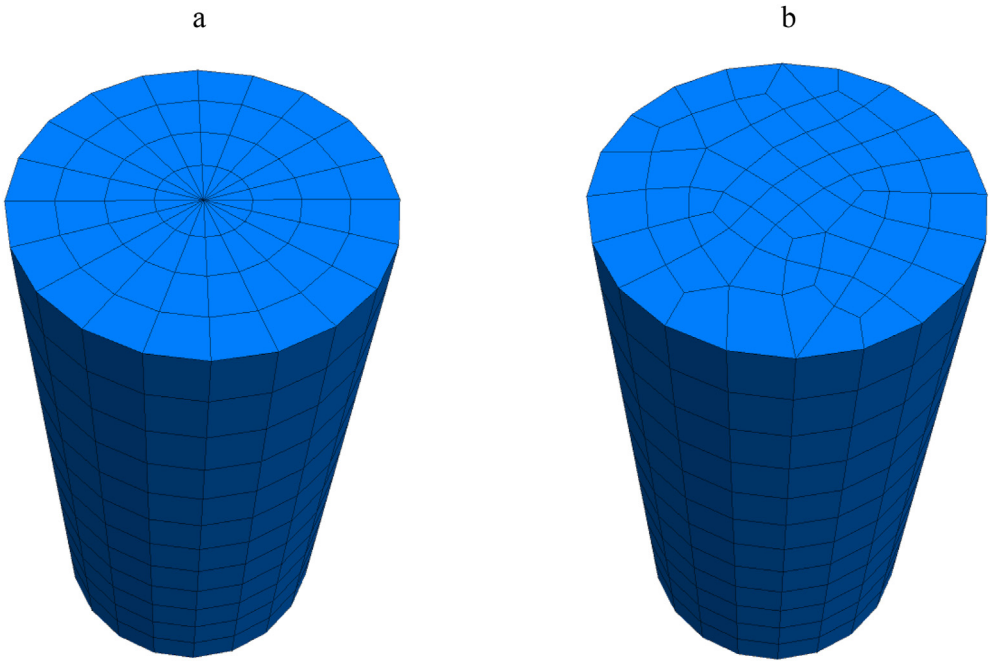

Fig. 4. An example of a mesh shape with an average zone length of 10 mm a) mesh pattern I, b) mesh pattern II.

Table 3. Number of zones due to mesh patterns and the average zone length.

Average zone length, mm	10	5	3	1.5
Mesh pattern I	960	6720	22,800	204,800
Mesh pattern II	792	5976	22,480	202,320

physical instability, the path dependency of nonlinear materials, and the nonlinearity of the stress–strain response. A constitutive model introduces and describes the stress–strain behaviour in response to applied loads relevant to post-failure. This model is used to predict the plastic and elastic straining of the material and the physical properties of a given material [33]. In pre-failure, most constitutive models have simple linear elastic behaviour, and complexity occurs in the post-failure region. So the rate of change of the strength of the material is a significant factor and should be considered in modelling the materials [45]. The behaviour of rock materials generally evolves in three possible ways

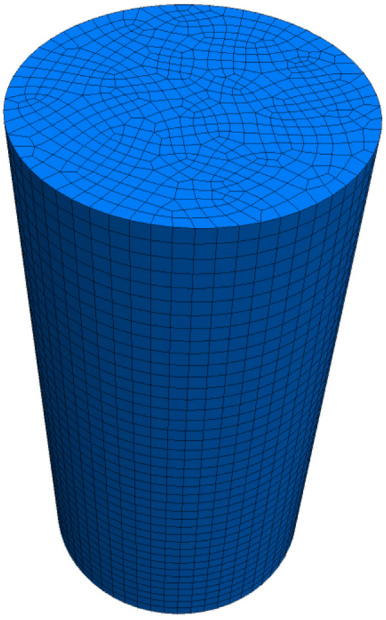

Fig. 5. Final mesh designing with an average zone length of 3 mm.

Table 4. Yield strength value due to mesh pattern and the average zone length.

Mesh pattern I			Mesh pattern II		
Average zone length, mm	Yield strength, Pa	Relative error in the number of zones, %	Average zone length, mm	Yield strength, Pa	Relative error in the number of zones, %
1.5	32,264,700	0	1.5	32,190,700	0
3	32,109,200	0.482	3	32,099,900	0.282
5	32,108,900	0,483	5	32,080,500	0.342
10	32,069,100	0,606	10	32,017,700	0.537

Table 5. Built-in plastic constitutive models in FLAC3D [33].

Constitutive model	Representative material	Example application
Mohr-Coulomb	Loose and cemented granular material: soils, rocks, concrete	General soil and rock mechanics
Ubiquitous joint	Laminated material with strength anisotropy	Excavation in closely bedded strata
Strain-softening	Granular material that exhibits nonlinear material hardening or softening	Studies in post-failure

related to the unstable physical system. A hard, good-quality rock material tends to show an elastic-brittle behaviour, in which the strength drops rapidly once the material is introduced to plastic straining. An averagequality rock material tends to show a strain-softening behaviour after the failure occurred. It has been assumed that post-failure deformation occurs at a constant stress level, defined by the compressive strength of the broken rock mass. A very poor quality rock material shows an elastic-perfectly plastic behaviour. This means that it continues to deform at a constant stress level and that no volume change is associated with this ongoing failure [38,46]. A consequence of the nonlinearity of the stress–strain relations caused by failure criteria is categorised in a plastic group. The different models are characterised by their yield function, hardening/softening functions and plastic flow. The plastic flow formulation is based on basic assumptions that the total strain may be divided into elastic and plastic parts. The flow rule specifies the plastic strain increment vector's direction as that normal to the potential surface. Different plasticity models are classified based on shear yield, potential functions, non-associated flow rules, and stress corrections [33].

In FLAC3D, there are 15 basic mechanical constitutive models provided in Version 5.0 including 1 null model, 3 elastic models and 11 plastic models. The choice of a constitutive model, depends on the characteristics of modelled material and the intended application of the constitutive model [33]. The potential constitutive plastic models taken into consideration to simulate the uniaxial compression test are summarised in Table 5.

In the numerical simulation, the mechanical parameters of the selected constitutive models were calibrated to obtain such results that matched the laboratory testing results. The mechanical parameters of siltstone adopted for modelling are based on the laboratory results, as shown in Table 2. The basic mechanical parameters of the strain-softening model and ubiquitous joint model are based on the Mohr-Coulomb model. In addition, the plastic strain parameter at the residual strength e_p and the mechanical parameters of the weakness plane (joint friction angle, joint cohesion, joint tension limit) will be adopted and simulated for the strain-softening model and the ubiquitous joint model, relatively.

4. Results comparison and discussions

The simulation results were presented in the form of stress–strain plots and contours of shear-strain rate indicating failure (fracture) of the sample. Due to the large number of results, only selected maps for individual models are shown. Elastic parameters of the cylindrical sample were adopted based on the results of the laboratory tests given in Table 2.

4.1. Mohr-Coulomb model

Compression simulation was conducted for the classic Mohr-Coulomb model with different shear strength sets given in Table 6. The value of friction angle and cohesion were calculated due to formula (1) of compressive strength [47]:

$$\sigma_c = 2c\sqrt{\frac{1+\sin\theta}{1-\sin\theta}} \tag{1}$$

where σ_c – compressive strength, c – cohesion, θ - friction angle

Stress–strain plots and fracture patterns for compression of Mohr-Coulomb sample with different shear strength set are shown in Fig. 6.

Table 6. Mechanical parameters of the Mohr-Coulomb model adopted for modelling.

Bulk modulus, K (GPa)	Shear modulus, G (GPa)	Friction angle, θ (deg.)	Cohesion, c (MPa)	Tensile strength, R_t (MPa)
10	8.5	30	9.2	3.2
		35	8.3	
		40	7.5	
		45	6.6	

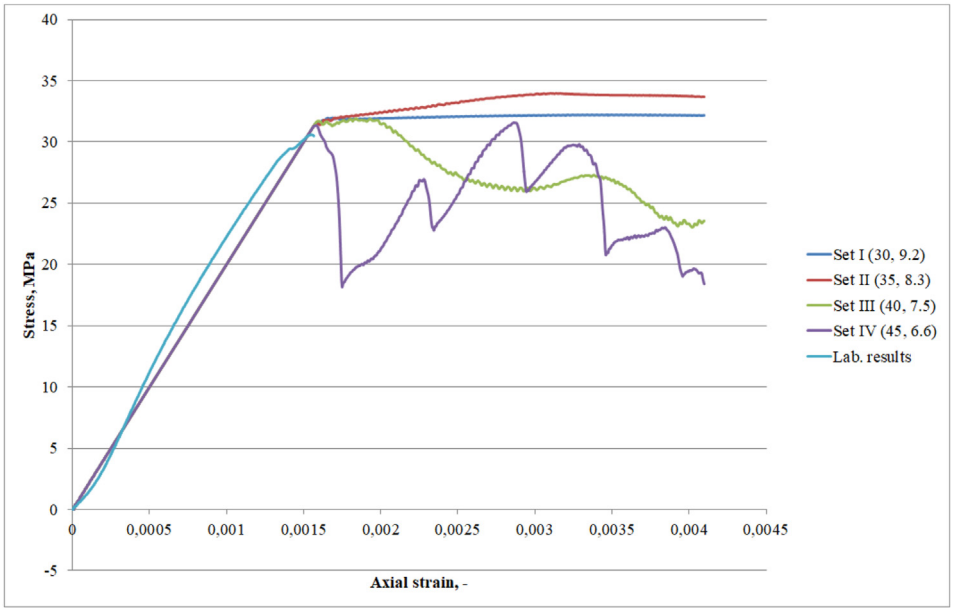

Fig. 6. Stress–strain plots comparison for compression of Mohr-Coulomb sample with different shear strength set.

Elastic region plots for all sets are identical and matched with the laboratory results; however, post-failure (plastic region) behaviours differ. The fracture pattern for set III seems to be the closest one to the laboratory fracture pattern (Fig. 7). Results comparison indicates that the best match is the shear strength set with the cohesion of 7.5 MPa and friction angle of 40 deg.

In the next step, the best-match strength parameters were reduced and recalculated in order to

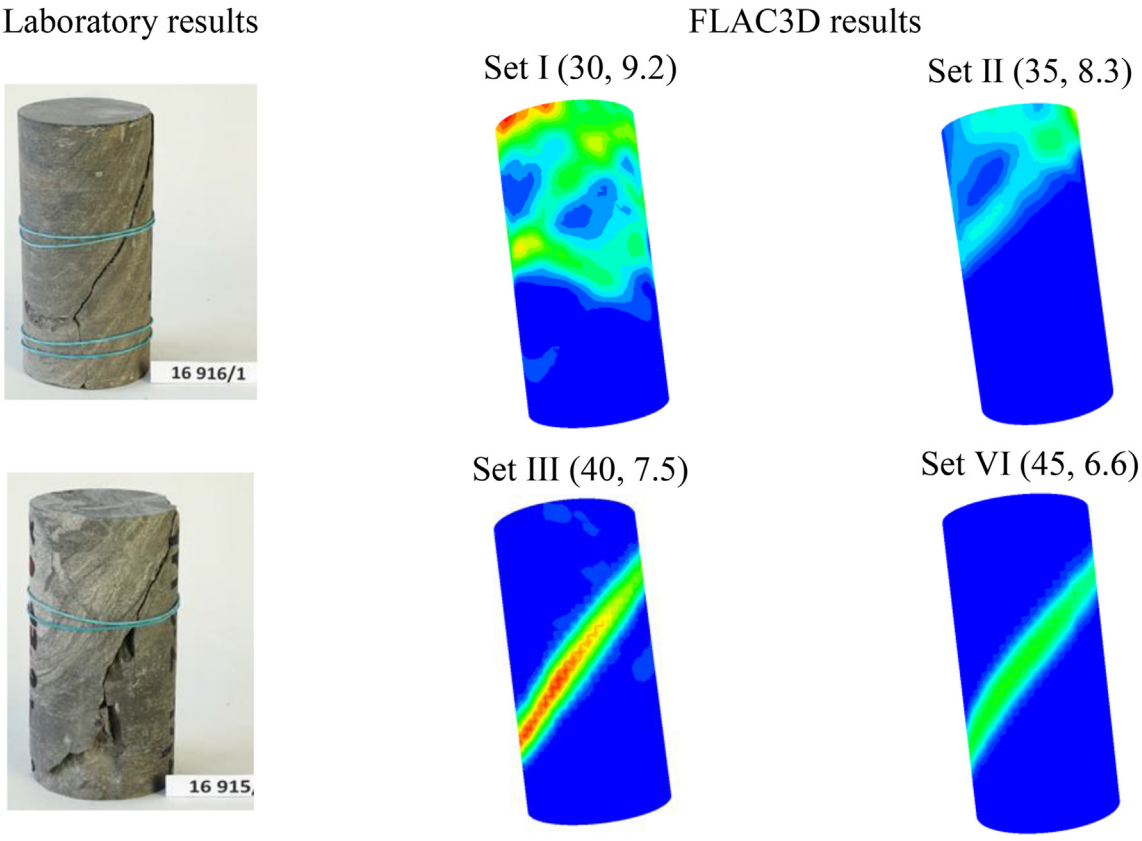

Fig. 7. Fracture pattern comparison for compression of Mohr-Coulomb sample with different shear strength set.

a

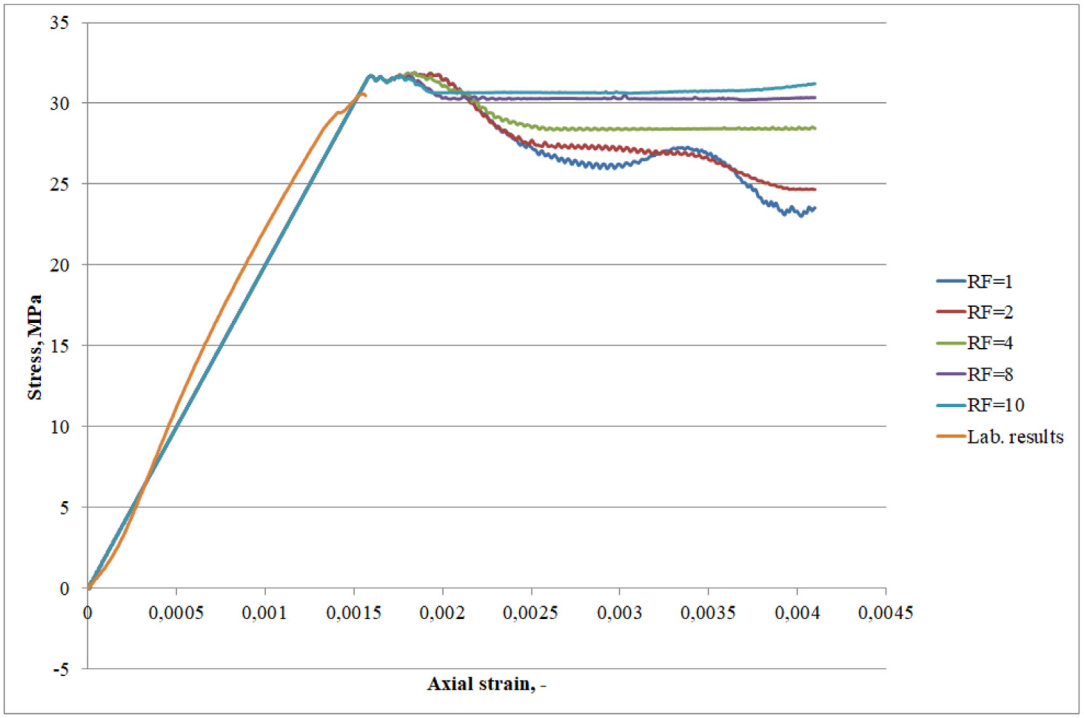

b

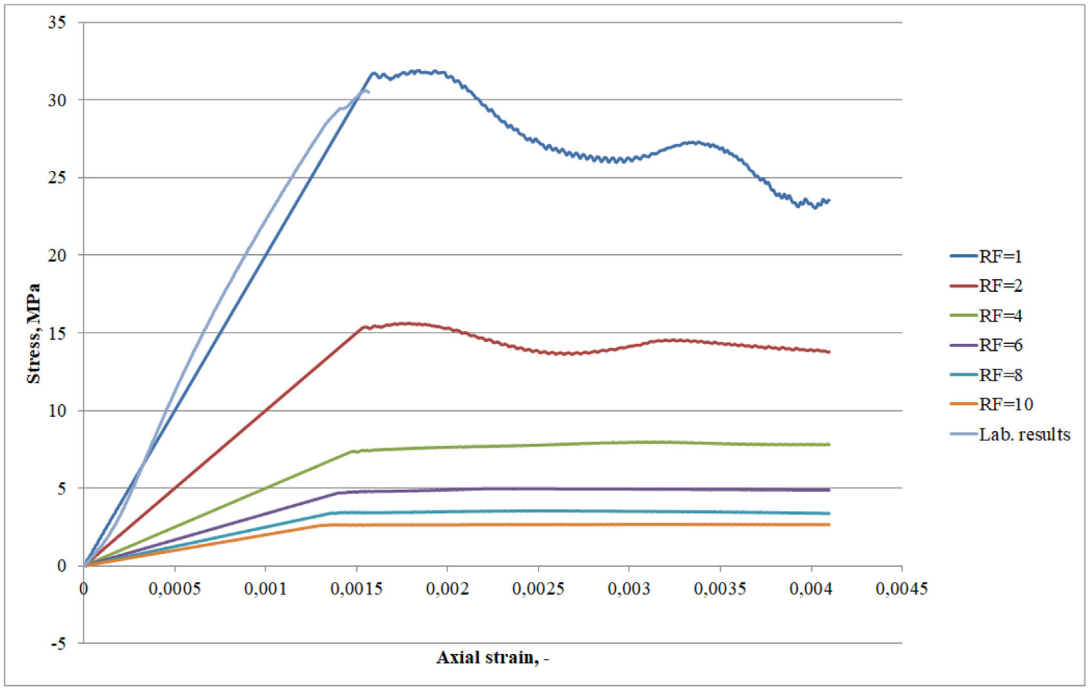

Fig. 8. Stress–strain plots comparison for compression of Mohr-Coulomb sample with Reduction Factor (RF): a) for only tensile strength (RF=1, 2, 4, 8, 10); b) for both strain and strength parameters (RF=1, 2, 4, 6, 8, 10).

match the laboratory fracture pattern. Stress–strain plots for compression of the Mohr-Coulomb sample with the Reduction Factor (RF) are shown in Fig. 8.

Reduction of tensile strength only: FLAC3D results are close to the laboratory results in the elastic region. Tensile strength has only an impact on the plastic region of the sample. Fracture patterns were not matched the laboratory fracture pattern. Reduction of strain and strength simultaneously: with the unreduced (RF = 1), FLAC3D results are close to the laboratory results. With the adopted RF, FLAC3D results show the lower yield strength

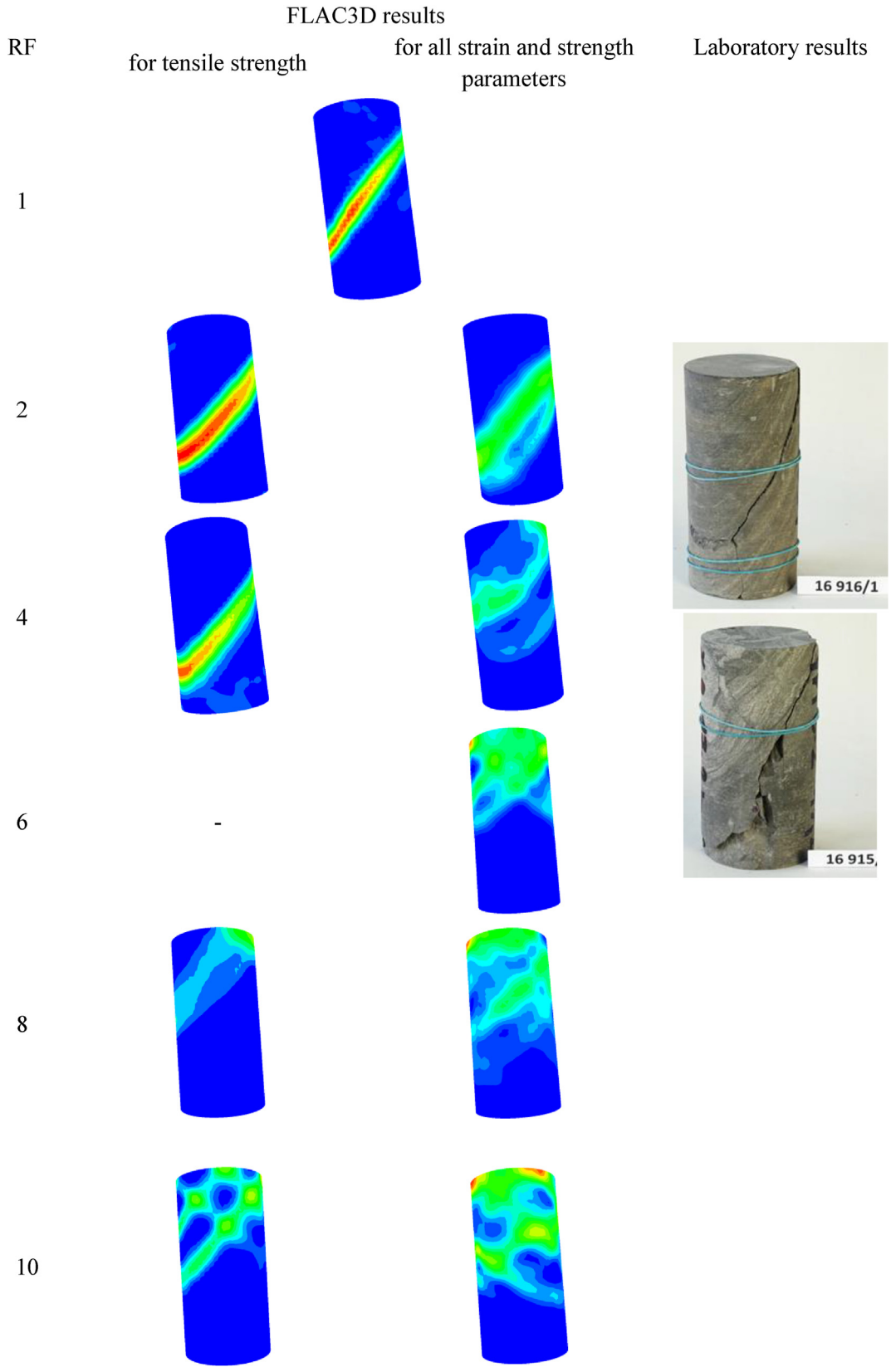

Fig. 9. Fracture pattern comparison for compression of Mohr-Coulomb sample.

Table 7. Simulation variations for compression of strain-softening Mohr-Coulomb sample.

Values of the residual strength	Values of plastic strain parameter at the residual strength		
	0.001	0.005	0.010
−25%	I	II	III
−50%	IV	V	VI
−75%	VII	VIII	IX

of the sample. In the case of RF = 6, 8, 10, the behaviour of the sample is close to perfectly plastically behaviour. These results are not matched with the laboratory results. Fracture pattern comparison also confirmed such a tendency of sample behaviour. The FLAC3D fracture patterns are way different from the laboratory fracture pattern (Fig. 9).

Based on the analysis of the results, the Mohr-Coulomb model can be considered inappropriate for modelling the given uniaxial compressive strength laboratory test.

4.2. Strain-softening Mohr-Coulomb model

Stress–strain plots for compression of strain-softening Mohr-Coulomb sample with different values of the residual strength and values of plastic strain parameter at the residual strength (Table 7).

Simulation variations shown in Table 7 were run for the shear-softening sample, tensile-softening sample and both shear- and tensile-softening samples.

An example of stress–strain plots for compression of shear-softening Mohr-Coulomb sample is shown in Figs. 10 and 11.

FLAC3D results are close to the laboratory results in the elastic region. However, fracture patterns were not matched the laboratory fracture pattern. The same tendency was obtained for the compression of the tensile-softening sample and both shear- and tensile-softening samples. Hence, the strain-softening model can also be considered inappropriate for modelling the given uniaxial compressive strength laboratory test.

4.3. Ubiquitous joint Mohr-Coulomb model

Compression simulation was conducted for the ubiquitous joint Mohr-Coulomb model with different shear strength sets of a weak plane given in Table 8. Values of friction angle and cohesion of weak plane were calculated due to the following formulas (2) and (3) [47]:

$$\sigma_c = \frac{2c_j}{k \cdot \sin 2\beta} \tag{2}$$

$$k = 1 - \tan\theta_j \cdot \tan\beta \tag{3}$$

where: β is the weak plane angle, c_j and θ_j are the cohesion and friction angle of weak plane.

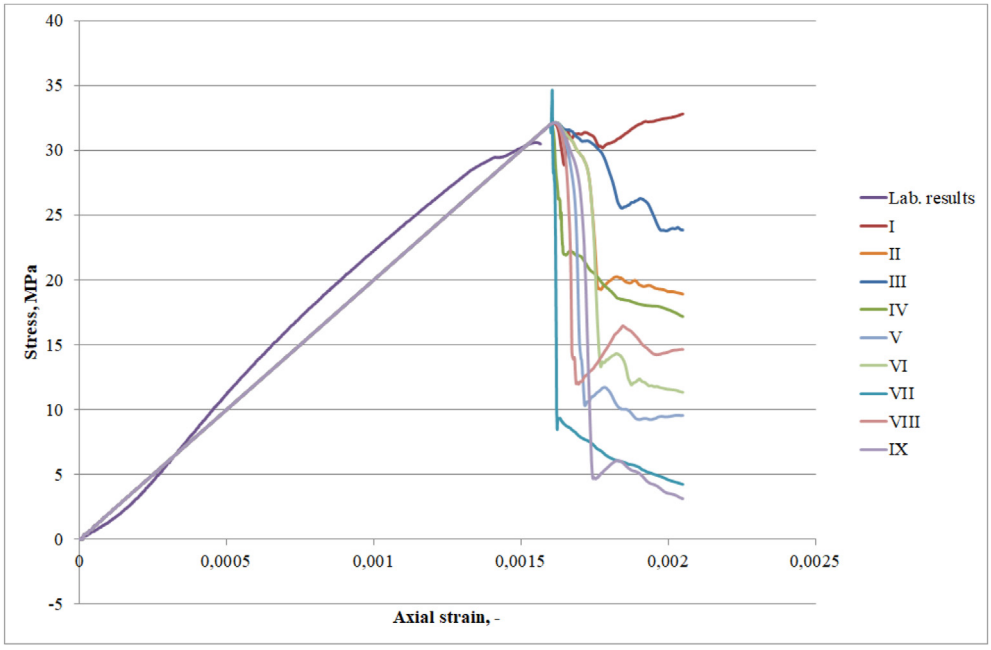

Fig. 10. Stress–strain plots for compression of shear-softening Mohr-Coulomb sample.

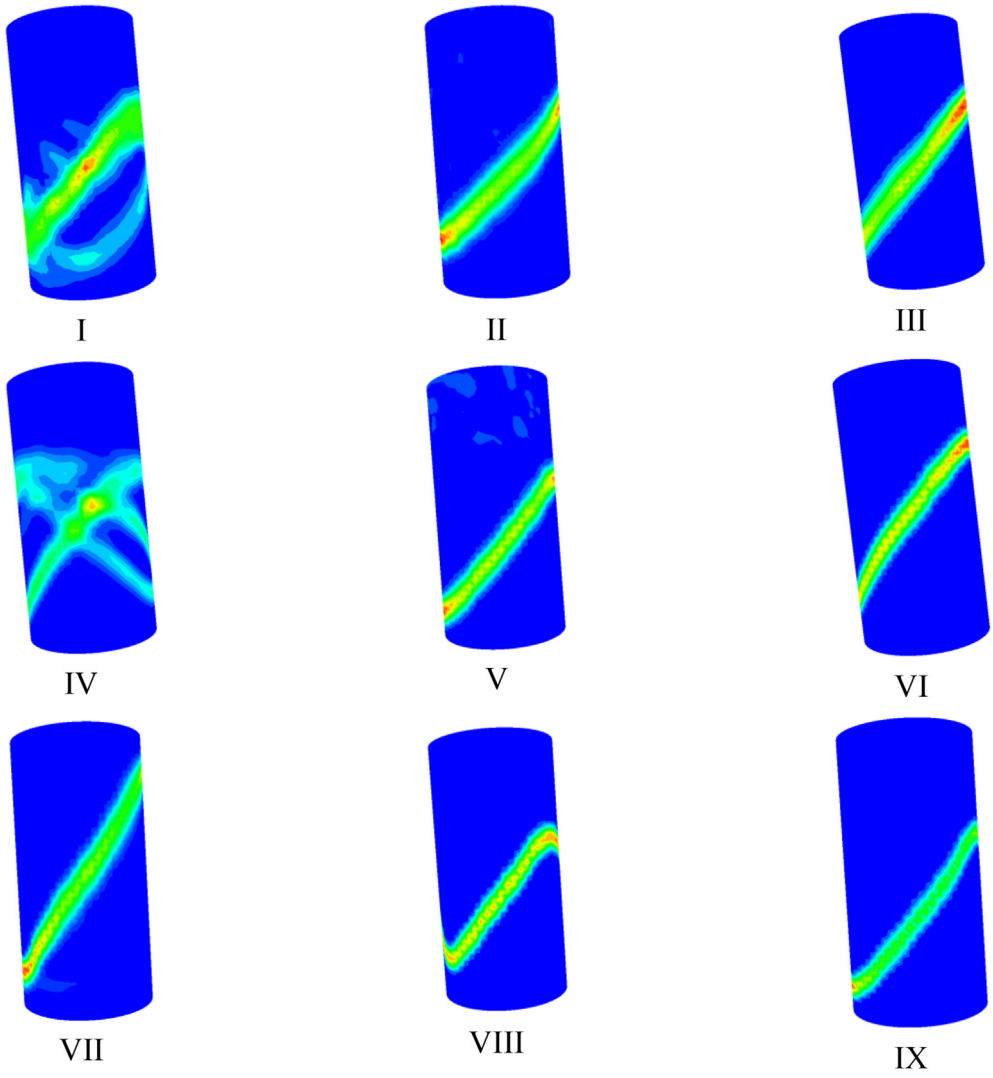

Fig. 11. Fracture pattern comparison for compression of shear-softening Mohr-Coulomb sample.

Stress–strain plots indicate that FLAC3D results were close to the laboratory results in the case of high shear strength of a weak plane (variation V) (Fig. 12). However, the FLAC3D fracture patterns were closed in case of low shear strength of a weak plane (I and II) (Fig. 13). To find the compromise case to match the FLAC3D results and the laboratory results, simulations were carried out for low friction angle – high cohesion and high friction angle – low cohesion. The best case is shown in Fig. 14. Values of shear strength were 24 deg. of friction angle and 5.5 MPa of cohesion. The FLAC3D results were in good agreement with the laboratory results in term of Stress–strain plot and major fracture plane. However, it still cannot model the micro-cracks that occurred in the laboratory tests.

Table 8. Shear strength sets of a weak plane for modelling (for the weak plane angle of 70 deg.).

Shear strength of weak plane	I	II	III	IV	V
c_j, MPa	2.3	3.5	4.7	6	7.3
θ_j, deg.	24	26	28	30	32

Ubiquitous joint model can be considered appropriate for modelling the given uniaxial compressive strength laboratory test. The mechanical parameters of the rock sample and the weak plane can be calibrated and defined after the results matching the Stress–strain plot and the macro fracture pattern of the given rock sample.

In general, all selected constitutive models managed to model the elastic behaviour (pre-failure) of a rock sample by adopting the deformation parameters (Young's modulus and Poisson's ratio)

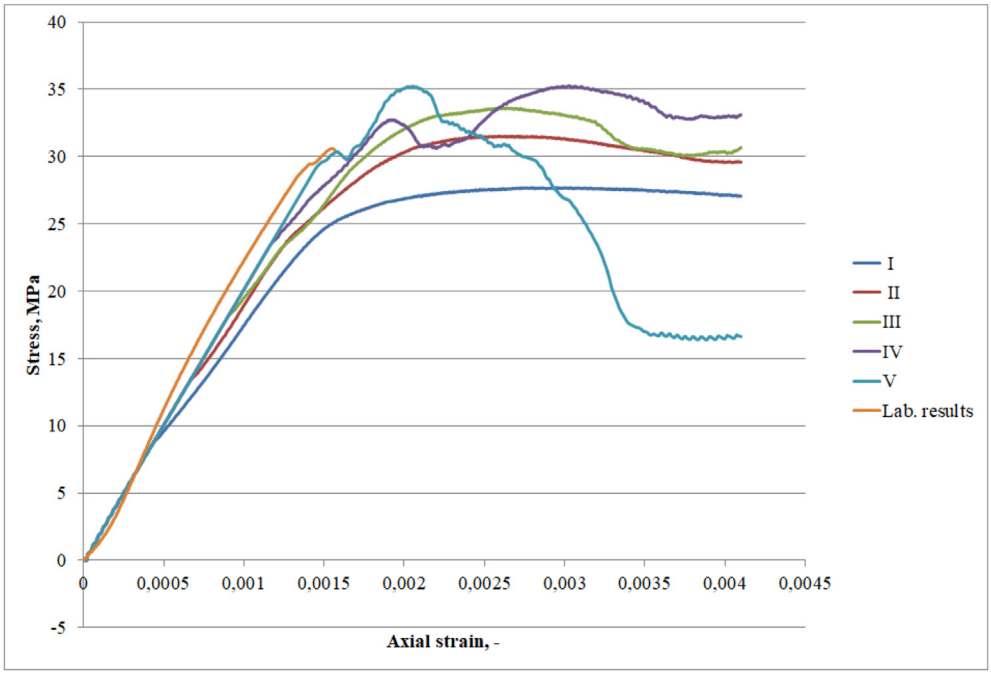

Fig. 12. Stress–strain plots comparison for compression of ubiquitous joint Mohr-Coulomb sample with different shear strength sets of a weak plane.

obtained from the laboratory tests. The fracture pattern that occurred in the laboratory tests was not fully modelled. None of the selected constitutive models did manage to model the micro-fractures due to the heterogeneity of natural rocks. Technically, it is possible to model these micro-fracture parameters or create a new constitutive model including all detailed parameters. However, many

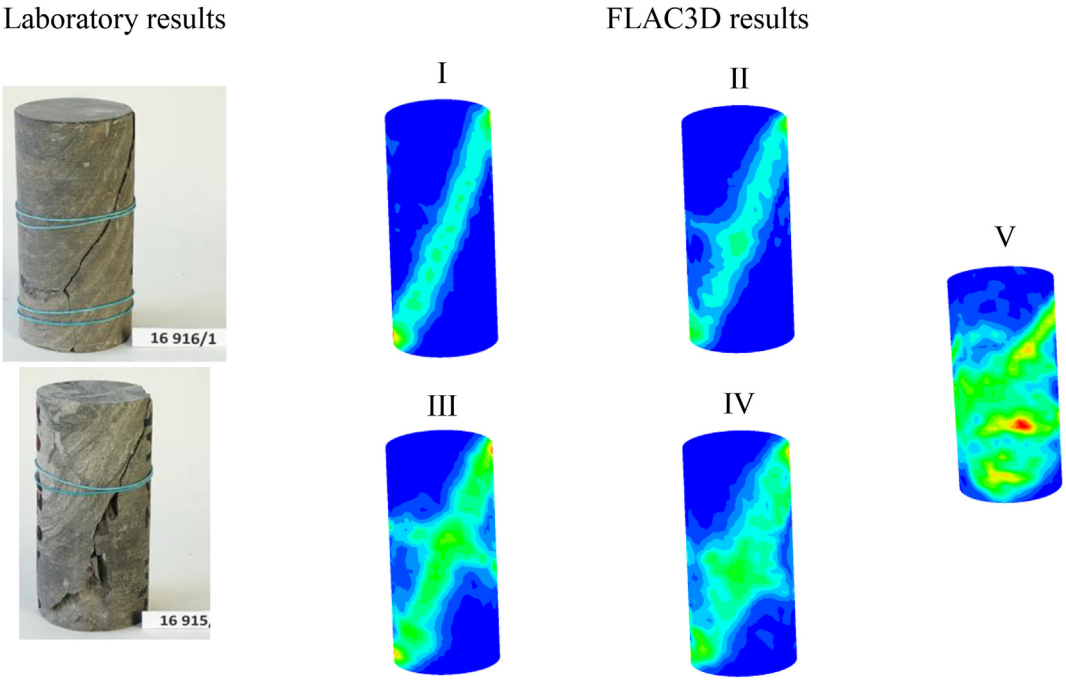

Fig. 13. Fracture pattern comparison for compression of ubiquitous joint Mohr-Coulomb sample with different shear strength sets of a weak plane.

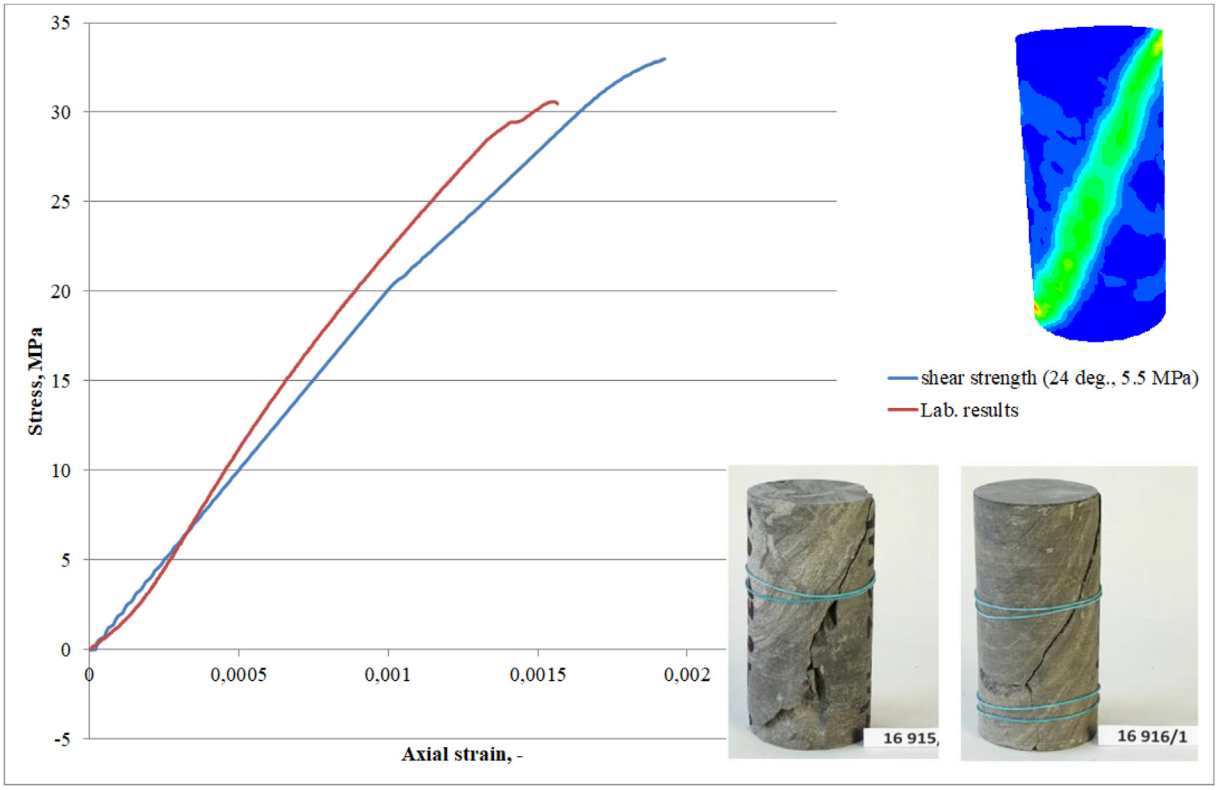

Fig. 14. The FLAC3D results and the laboratory results in good agreement for compression of ubiquitous joint Mohr-Coulomb sample.

micro-fracture parameters cannot be easily measured or determined. Moreover, taking all the complex parameters into account would make the calibration an over-determined issue. Only the ubiquitous joint constitutive model managed to model the macro-fracture of rock samples. Therefore, the ubiquitous joint constitutive model is considered an appropriate constitutive model that fulfils expectations of the research purpose.

5. Conclusions

Dozens of simulations of the cylindrical sample compression were carried out using FLAC3D, taking different constitutive models and their mechanical parameters into consideration in order to model the uniaxial compression test of rock samples (siltstone). Based on the results, some conclusions can be drawn.

- Constitutive models and their input properties have played an important role in the final results. It has also confirmed in other studies.
- The elastic behaviour (pre-failure) of the rock sample can be modelled by using all selected constitutive models. However, the fracture mode (post-failure) was not fully modelled. Only ubiquitous joint constitutive model managed to model the macro fracture of the rock sample by assuming the weak plane with an adequate angle.
- In the case of the ubiquitous joint constitutive model, the strength parameters of the rock sample and the shear strength of weak plane can be approximately determined.
- All selected constitutive models failed to fully represent the microscale fractures of samples that occurred in laboratory testing. It should be noted that rock mass is a natural heterogeneous structure, and the rock samples vary from each other due to composition and the orientation of the lamination. Further studies should be focused on this aspect to improve and verify the results of such a case of modelling.
- Laboratory results are not so common for the estimation of post-failure parameters. Research on the post-failure behaviour of rocks should be conducted and reported in order to verify and confirm the modelling results.
- This study is expected to provide a reference for other cases of modelling of UCS laboratory tests.

Ethical statement

The authors state that the research was conducted according to ethical standards.

Funding body

This research received no external funding.

Conflicts of interest

The authors declare no conflict of interest.

References

[1] Bieniawski ZT, Bernede MJ. Suggested methods for determining the uniaxial compressive strength and deformability of rock materials: Part 1. Suggested method for determination of the uniaxial compressive strength of rock materials. Int J Rock Mech Min Sci 1979;16(2):137–8.
[2] Bieniawski ZT, Bernede MJ. Suggested methods for determining the uniaxial compressive strength and deformability of rock materials: Part 2. Suggested method for determination deformability of rock materials in uniaxial compression. Int J Rock Mech Min Sci 1979;16(2):138–40. https://doi.org/10.1016/0148-9062(79)91451-7.
[3] Goodman RE. Introduction to rock mechanics. 2nd ed. London: Wiley; 1989.
[4] Brady BHG, Brown ET. Rock mechanics for underground mining. New York: Kluwer Academic Publish; 2004.
[5] Bieniawski ZT. Mechanism of brittle fracture of rock: Part I—theory of the fracture process. Int J Rock Mech Min Sci Sciences & Geomechanics Abstracts. 1967;4(4):395–404. https://doi.org/10.1016/0148-9062(67)90030-7.
[6] Martin CD, Chandler NA. The progressive fracture of Lac du Bonnet granite. Int J Rock Mech Min Sci Sciences and Geomechanics Abstracts 1994;31(6):643–59. https://doi.org/10.1016/0148-9062(94)90005-1.
[7] Li L, Lee PKK, Tsui Y, Tham LG, Tang CA. Failure process of granite. Int J Geom 2003;3(1):84–98. https://doi.org/10.1061/(ASCE)1532-3641(2003)3:1(84).
[8] Szwedzicki T. A hypothesis on modes of failure of rock samples tested in uniaxial compression. Rock Mech Rock Eng 2007;40(1):97–104. https://doi.org/10.1007/s00603-006-0096-5.
[9] Wong LNY, Einstein HH. Systematic evaluation of cracking behavior in specimens containing single flaws under uniaxial compression. Int J Rock Mech Min Sci 2009;46(2):239–49. https://doi.org/10.1016/j.ijrmms.2008.03.006.
[10] Pu CZ, Cao P. Failure characteristics and its influencing factors of rock-like material with multi-fissures under uniaxial compression. Trans Nonferrous Metals Soc China 2012;22(1):185–91. https://doi.org/10.1016/S1003-6326(11)61159-X.
[11] Basu A, Mishra DA, Roychowdhury K. Rock failure modes under uniaxial compression, Brazilian, and point load tests. Bull Eng Geol Environ 2013;72:457–75. https://doi.org/10.1007/s10064-013-0505-4.
[12] Eberhardt E, Stead D, Stimpson B, Read RS. Identifying crack initiation and propagation thresholds in brittle rock. Can Geotech J 1998;35(2):222–33. https://doi.org/10.1139/cgj-35-2-222.
[13] Xu H, Qin Y, Wang G, Fan C, Wu M, Wang R. Discrete element study on mesomechanical behavior of crack propagation in coal samples with two prefabricated fissures under biaxial compression. Powder Technol 2020;375:42–59. https://doi.org/10.1016/j.powtec.2020.07.097.
[14] Chen W, Wan W, Zhao Y, Peng W. Experimental study of the crack predominance of rock-like material containing parallel double fissures under uniaxial compression. Sustainability 2020;12(12):5188. https://doi.org/10.3390/su12125188.
[15] Bobet A, Einstein HH. Fracture coalescence in rock-type materials under uniaxial and biaxial compression. Int J Rock Mech Min Sci 1998;35(7):863–88. https://doi.org/10.1016/S0148-9062(98)00005-9.
[16] Morgan SP, Einstein HH. The effect of bedding plane orientation on crack propagation and coalescence in shale. In: 48th US rock mechanics/geomechanics symposium. Minneapolis, Minnesota: American Rock Mechanics Association; 2014.
[17] Stefanizzi S, Barla GB, Grasselli G. Numerical modelling of standard rock mechanics laboratory tests using a finite/discrete element approach. In: 3. Canada-US rock mechanics symposium; 20. Canada rock mechanics symposium; 2009. Toronto, Canada.
[18] Mahabadi O, Kaifosh P, Marschall P, Vietor T. Three-dimensional FDEM numerical simulation of failure processes observed in Opalinus Clay laboratory samples. J Rock Mech Geotech Eng 2014;6(6):591–606. https://doi.org/10.1016/j.jrmge.2014.10.005.
[19] Tatone BSA, Grasselli G. A calibration procedure for two-dimensional laboratory-scale hybrid finite–discrete element simulations. Int J Rock Mech Min Sci 2015;75:56–72. https://doi.org/10.1016/j.ijrmms.2015.01.011.
[20] Mardalizad A, Scazzosi R, Manes A, Giglio M. Testing and numerical simulation of a medium strength rock material under unconfined compression loading. J Rock Mech Geotech Eng 2018;10(2):197–211. https://doi.org/10.1016/j.jrmge.2017.11.009.
[21] Xiong LX, Chen HJ, Geng DX. Uniaxial compression study on mechanical properties of artificial rock specimens with cross-flaws. Geotech Geol Eng 2021;39:1667–81. https://doi.org/10.1007/s10706-020-01584-z.
[22] Xiong LX, Yuan HY, Zhang Y, Zhang KF, Li JB. Experimental and numerical study of the uniaxial compressive stress–strain relationship of a rock mass with two parallel joints. Arch Civ Eng 2019;65(2):67–80. https://doi.org/10.2478/ace-2019-0019.
[23] Oliveira MM, Pinto CLL, Mazzinghy DB. FEM-DEM simulation of Uniaxial Compressive Strength (UCS) laboratory tests. Int Eng J 2020;73(4):561–9. https://doi.org/10.1590/0370-44672019730078.
[24] Pajak M, Baranowski P, Janiszewski J, Kucewicz M, Mazurkiewicz L, Łaźniewska-Piekarczyk B. Experimental testing and 3D meso-scale numerical simulations of SCC subjected to high compression strain rates. Construct Build Mater 2021;302(6):124379. https://doi.org/10.1016/j.conbuildmat.2021.124379.
[25] Kucewicz M, Baranowski P, Małachowski J. Dolomite fracture modelling using the Johnson-Holmquist concrete material model: parameter determination and validation. J Rock Mech Geotech Eng 2021;13(2):335–50. https://doi.org/10.1016/j.jrmge.2020.09.007.
[26] Kucewicz M, Baranowski P, Małachowski J. Determination and validation of Karagozian-Case Concrete constitutive model parameters for numerical modeling of dolomite rock. Int J Rock Mech Min Sci 2020;129(7):104302. https://doi.org/10.1016/j.ijrmms.2020.104302.
[27] Li H, Wong L. Influence of flaw inclination angle and loading condition on crack initiation and propagation. Int J Solid Struct 2012;49(18):2482–99. https://doi.org/10.1016/j.ijsolstr.2012.05.012.
[28] Yang SQ, Huang YH, Jing HW, Liu XR. Discrete element modeling on fracture coalescence behavior of red sandstone containing two unparallel fissures under uniaxial compression. Eng Geol 2014;178:28–48. https://doi.org/10.1016/j.enggeo.2014.06.005.
[29] Bahaaddini M, Hagan PC, Mitra R, Hebblewhite BK. Scale effect on the shear behaviour of rock Joints based on a numerical study. Eng Geol 2014;181:212–23. https://doi.org/10.1016/j.enggeo.2014.07.018.
[30] Zhao W, Huang R, Yan M. Mechanical and fracture behaviour of rock mass with parallel concentrated joints with

different dip angle and number based on PFC simulation. Geomechanics and Engineering 2015;8(6):757–67. https://doi.org/10.12989/gae.2015.8.6.757.
[31] Haeri H, Sarfarazi V, Zhu Z, Nejati HR. Numerical simulations of fracture shear test in anisotropy rocks with bedding layers. Advances in Concrete Construction 2019;7(4):241–7. https://doi.org/10.12989/acc.2019.7.4.241.
[32] Zhang L, Zhu J. Analysis of mechanical strength and failure morphology of prefabricated closed cracked rock mass under uniaxial compression. Geotech Geol Eng 2020;38:4905–15. https://doi.org/10.1007/s10706-020-01335-0.
[33] Itasca Consulting Group Inc. FLAC3D (3-dimensional finite difference software). Software available at:. 2012. Minneapolis, Version 5.0. www.itascacg.com.
[34] Čsn EN. 1926 (72 1142) Zkušební metody přírodního kamene - stanovení pevnosti v prostém tlaku. Český normalizační institut. ICS 73.20; 91.100.15, Červenec 2007 [In Czech)].
[35] Deere DU. Rock quality designation (RQD) after twenty years. Contract Report GL-89-1. Washington, D.C.: U.S. Army Corps of Engineers; 1989.
[36] Deere DU, Deere DW. The rock quality designation (RQD) index in practice. In: Proceedings of the symposium rock classification systems for engineering purposes, ASTM Special Publication 984, American Society for Testing and Materials; 1988. p. 91–101. Philadelphia.
[37] Bieniawski ZT. Engineering rock mass classifications: a complete manual for engineers and geologists in mining, civil and petroleum engineering. New York: John Wiley and Sons, Inc.; 1989.
[38] Hoek E, Brown ET. Practical estimates of rock mass strength. Int J Rock Mech Min Sci 1997;34(8):1165–86. https://doi.org/10.1016/S1365-1609(97)80069-X.
[39] Kucewicz M, Baranowski P, Małachowski J. Determination and validation of Karagozian-Case Concrete constitutive model parameters for numerical modeling of dolomite rock. Int J Rock Mech Min Sci 2020;129:104302. https://doi.org/10.1016/j.ijrmms.2020.104302.
[40] Bomers A, Schielen RMJ, Hulscher SJMH. The influence of grid shape and grid size on hydraulic river modelling performance. Environ Fluid Mech 2019;19:1273–94. https://doi.org/10.1007/s10652-019-09670-4.
[41] Guo L, Xiang J, Latham JP, Izzuddin B. A numerical investigation of mesh sensitivity for a new three-dimensional fracture model within the combined finite-discrete element method. Eng Fract Mech 2016;151:70–91. https://doi.org/10.1016/j.engfracmech.2015.11.006.
[42] Dutt A. Effect of mesh size on finite element analysis of beam. SSRG Int J Mech Eng 2015;2(12):8–10. https://doi.org/10.14445/23488360/IJME-V2I12P102.
[43] Abbasi B, Russell D, Taghavi R. FLAC3D mesh and zone quality. Continuum and distinct element numerical modeling in geomechanics. In: Zhu Detournay, Hart, Nelson, editors. Paper: 11-02. Minneapolis: Itasca International Inc.; 2013.
[44] Preh A, Illeditsch M. The perfect mesh for FLAC3D to analyse the stability of rock slopes. In: Conference: 4th international FLAC symposium on numerical modelling in geomechanics; 2006. Madrid, Spain.
[45] Strafield M, Cundall P. Towards a methodology for rock mechanics modelling. Int J Rock Mech Min Sci 1988;25(3):99–106. https://doi.org/10.1016/0148-9062(88)92292-9.
[46] Smed EM, Cundall P. Elasto-plasto strain hardening mohr-coulomb model-derivation and implementation. Denmark: Aalborg; 2012.
[47] Jaeger JC, Cook NGW. Fundamentals of rock mechanics. 3rd ed. NewYork: Chapman & Hall; 1979.